Galdeano-Ruano, CP.; Wittee Lopes, C.; Motta Meira, D.; Corma Canós, A.; Oña-Burgos, P. (2021). Rh2P Nanoparticles Stabilized by Carbon Patches for Hydroformylation of Olefins. ACS Applied Nano Materials. 4(10):10743-10753. https://doi.org/10.1021/acsanm.1c02194

Rh_2P Nanoparticles Stabilized by Carbon Patches for Hydroformylation of Olefins

Carmen Galdeano-Ruano[1], Christian Wittee Lopes[2], Debora Motta Meira[3,4], Avelino Corma[1] and Pascual Oña-Burgos*[,1,5]

[1]*Instituto de Tecnología Química, Universitat Politècnica de València-Consejo Superior de Investigaciones Científicas (UPV-CSIC), Avda. de los Naranjos s/n, 46022 Valencia, Spain.*

[2]*Laboratório de Reatividade e Catálise (LRC), Universidade Federal do Rio Grande do Sul, 91501-970 Porto Alegre, Brazil.*

[3]*CLS@APS, Advanced Photon Source, Argonne National Laboratory, 9700 S. Cass Avenue, Argonne, IL 60439, USA.*

[4]*Canadian Light Source Inc., 44 Innovation Boulevard, Saskatoon, Saskatchewan S7N 2V3, Canada.*

[5]*Department of Chemistry and Physics, University of Almería, Ctra. Sacramento, s/n, Almería, E-04120, Spain.*

ABSTRACT

One of the major challenges in science is the development of solid materials able to act as catalysts for chemical reactions that are commonly carried out using homogeneous molecular catalysts. In this sense, Rh_2P nanoparticles (NPs) have been identified as suitable mimics of $[Rh^{I}(Ph_3P)_3]^{+}$, the benchmark of homogeneous catalysts in liquid-phase hydroformylation. For this reason, a fitted synthetic strategy is required to develop catalysts based exclusively on Rh_2P NPs. In order to attain it, carbon-supported Rh_2P NPs have been prepared using two synthetic pathways, which differ in the Rh and P sources. In the first one, two separate sources of Rh and P were used. In the second one, the Wilkinson complex was employed as a unique source of Rh and P in order to probe the positive influence of the well-defined molecular organization on the preparation of dispersed and controlled Rh_2P nanoparticles after a pyrolysis treatment, which favours the

formation of carbon patches around the nanoparticle that stabilize it. In addition, metallic Rh nanoparticles were also synthesized to be used as reference. All catalysts have been compared by means of diverse characterization techniques such as transmission electron microscopy, X-ray diffraction and X-ray adsorption spectroscopy. The application of XAS to the study of Rh_2P NPs is unusual and has been essential in the discussion of the results.

Starting with a well-defined metal precursor leads to the exclusive formation of Rh_2P NPs with excellent catalytic activity for the liquid-phase hydroformylation. The role of P is to modulate the particle size and the electronic configuration of Rh species, resulting in the improvement of the catalytic performance and the obtention of turnover frequencies (TOFs) of 5236 h^{-1} at 60 ºC and 17788 h^{-1} at 100 ºC . Furthermore, the carbon present in the phosphine ligand favours nanoparticle stabilization by carbon patches during catalytic reaction.

Keywords: Rh_2P nanoparticles, heterogeneous catalysis, liquid-phase hydroformylation, XAS characterization, HRTEM.

Introduction

Hydroformylation, discovered in 1938 by Otto Roelen, is the transformation of olefins into aldehydes by H_2 and CO addition.[1] This reaction is an example of an atom economic process, in which all the starting materials are converted to products. Besides, it is one of the most important homogeneously catalysed industrial reactions. Aldehydes are valuable chemicals not only as final products but also as feedstock for the synthesis of amines, carboxylic acids and alcohols.[2,3] Catalyst separation and recovery[4] together with the high and voluble price of rhodium,[1] have boosted the research into heterogeneous catalysts able to carry out competitively the hydroformylation reaction. Important efforts have been performed on the development of heterogenous catalysts for this process. For instance, heterogenization of homogeneous hydroformylation catalysts on different supports, as porous organic polymers (POPs) made of vinyl functionalised phosphorus ligands[5,6] and composites of silica and organic polymers.[7] Besides, catalysts based on single atoms and nanoparticles supported on inorganic oxides such as

Al_2O_3,[8] CeO_2,[9] CoO,[10] mainly of metallic rhodium as active species, have shown promising results. Despite the significant role of phosphorus ligands in hydroformylation homogeneous catalysts,[11] little research has been done on the application of Rh phosphide catalysts in the mentioned reaction. Rh_2P nanoparticles have been used previously in catalysis, mostly in reactions involving hydrogen, such as hydrodeoxygenation,[12,13] hydrodesulfurization,[14–17] and the hydrogen evolution reaction.[18–20] In contrast to this, only two research works were found regarding the application of Rh_2P nanoparticles in hydroformylation, one in gas phase,[21] and another in liquid phase.[22]

Rh_2P has an antifluorite structure with a high metal to phosphorus ratio, which, compared to other phosphides, results in more metallic features, such as a Rh-Rh distance closer to metallic Rh. This effect has been theoretically proved after obtaining, with DFT calculations, projected density of states (PDOS) of surface Rh atoms, where the d-band centers of Rh, Rh_2P and RhP_2 have values of -1.40, -1.68 and -2.47 eV, respectively.[22] In these PDOS, Rh_2P showed peaks similar to those for $[Rh^I(Ph_3P)_3]^+$, revealing the similarity between the electronic structures of both species and shedding light on the potential of Rh_2P as heterogeneous catalysis in the hydroformylation of olefins.[22]

Although the synthesis of Rh_2P NPs has been attempted employing several approaches based on a rhodium metal precursor together with a phosphorus source under reducing atmosphere (H_2), a single Rh_2P phase was unfortunately never obtained.[21-22] Besides, these interesting works have widely studied the fresh catalytic material, but deeper insights into the stability of the spent catalyst with post-catalysis characterization are still needed. Based on that, herein, we report a straightforward, efficient and robust synthesis of exclusively Rh_2P nanoparticles, promoted through a commercially available source of Rh and P, the Wilkinson complex. Rh_2P nanoparticles were formed after incipient wetness impregnation on a carbon support and followed by pyrolysis under N_2 atmosphere, as we have achieved recently with a Co complex.[23] In this work, the aim is to report a selective and alternative method for forming nanoparticles based on single Rh_2P phase from a well-defined single precursor and contribute to the reported strategies for their

synthesis. In fact, these Rh_2P nanoparticles have shown a catalytic activity for hydroformylation comparable to the benchmark homogeneous catalyst with excellent stability of Rh_2P nanoparticles based on deep post-catalysis studies. In this sense, the XAS technique applied here to study Rh_2P NPs has been pivotal to prove the homogeneity of the fresh and spent materials.

Results and discussion

Carbon-supported Rh_2P nanoparticles with different Rh loadings were obtained after employing the Wilkinson complex as metal and phosphorus sources (Rh_2P@C). The preparation process of Rh_2P@C NPs is outlined in Scheme 1. Alternatively, another strategy was applied using $RhCl_3 \cdot xH_2O$ and PPh_3 as rhodium and phosphorus sources, respectively (Rh-PPh_3@C). Supported Rh^0 nanoparticles were also synthesized from $RhCl_3 \cdot xH_2O$ for comparison purposes (Rh@C). Catalyst preparation is described in the Supporting Information and the characterization results are presented below.

Scheme 1. Preparation process of Rh_2P@C NPs from the Wilkinson complex as single source of Rh and P

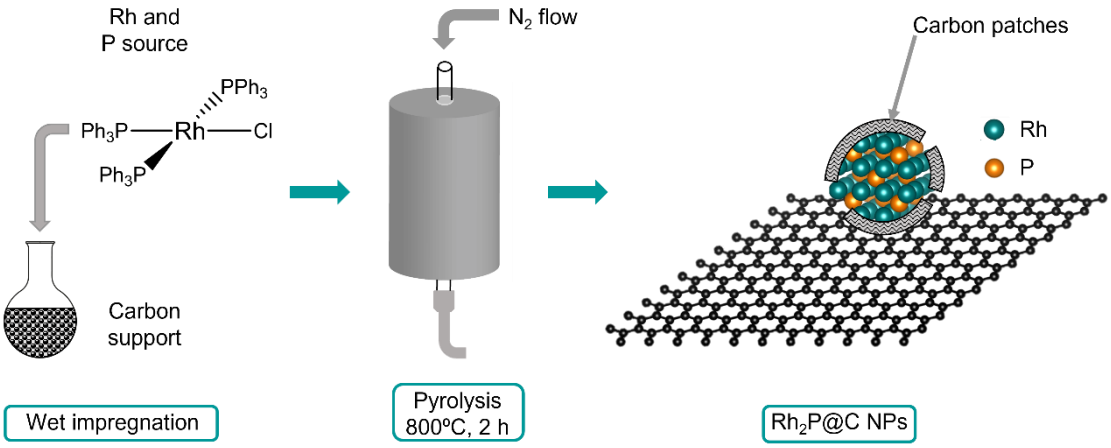

High-Angular Angle Dark-Field Scanning Transmission Electron Microscopy (HAADF-STEM) was used to study crystallinity, particle size and distribution for all catalysts, as these features may impact the catalytic performance. In Figure 1, representative STEM images are shown for 1%Rh_2P@C, 1%Rh-PPh_3@C and 1%Rh@C. Average particle sizes for these catalysts are very close: 2.1 nm for 1%Rh_2P@C, 2.1 nm for 1%Rh-PPh_3@C and 2.2 nm for 1%Rh@C. It should be noted that here, the pyrolysis temperature (800 ºC) did not seem to foster the formation of bigger

nanoparticles. This is consistent with our previous work, where materials were prepared at different temperatures of pyrolysis (400-800 ºC) and there were no evidence of particle growth at the highest temperature.[23] On the contrary, when the thermal treatment was performed in a stream of H_2 in Ar from 250 ºC to 900 ºC, Rh_2P particles in the range of 2 to 5 nm were obtained at lower temperature, while at the higher temperature, the average diameter raised up to 12 nm.[21]

In our case, HAADF-STEM results show that for Rh_2P@C at 5%, 1%, 0.5% and 0.3% Rh loadings, the particle mean sizes are 4.8, 2.1, 1.8 and 1.3 nm, respectively (Figures S1, S3, S4 and S5). There is a gradual decrease in the average diameter of Rh_2P@C materials when lowering the Rh content, and at 0.3% metal loading, the mean diameter became smaller and the particle size distribution was the narrower. Regarding catalysts prepared at 5% rhodium loading, the presence of phosphorus seems to promote the formation of smaller particles because 5%Rh@C particles have a diameter of 17.1 nm on average, with some of them as big as 30 nm; while 5%Rh_2P@C and 5%Rh-PPh_3@C (Figures S10, S3 and S8) underwent a less pronounced growth. This was also observed in a previous work of our group with nitrogenated ligands, which promoted the formation of smaller NPs than those without electron-donating ligands.[23] The catalyst preparation methods described here result in a better metal dispersion than reported before.[21-22]

Energy dispersive X-ray (EDX) and High-Resolution Transmission Electron Microscopy (HRTEM) revealed the presence of both phosphorus and rhodium in the same nanoparticles with 12.2% of phosphorus and 87.8% of rhodium for 1%Rh_2P@C, and 14.3% of P and 85.7% of Rh for 1%Rh-PPh_3@C (Figure S19 and Table S1). Among the possible rhodium phosphides that can be formed (Rh_2P, RhP_2, Rh_3P_2, Rh_4P_3, RhP_3), the result rules out the species RhP_2 and RhP_3, with theoretical weight percentages for Rh of 62.4% and 52.5%, respectively. Regarding Rh_3P_2, the weight percentages of Rh and P (83% and 17%) approach the values obtained here for 1%Rh_2P@C. However, the percentages of P and Rh determined experimentally are closer to the theoretical values for Rh_2P (13.1% of P and 86.9% of Rh) and the XRPD diffractogram of 5%Rh_2P@C discards the presence of Rh_3P_2 (Figure S25). HRTEM images were taken for 1%Rh_2P@C, 1%Rh-PPh_3@C, 1%Rh@C and 5%Rh_2P@C (Figure 1b and Figures S13-S18).

These images allowed d-spacing measurements of labeled lattice fringes, and in the case of 1%Rh_2P@C, distances were 1.4 Å, 2.0 Å and 2.8 Å, that were assigned to Rh_2P (400), (220) and (200), respectively. In order to prove that 1%Rh_2P@C and 5%Rh_2P@C share the same rhodium species, lattice spacing were also measured for the later and distances of 2.0 Å (220) and 2.8 Å (200) were obtained. Lattice measurements acquired for 1%Rh-PPh_3@C have values of 2.8 Å (200) and 1.2 Å (420), which correspond to Rh_2P species and are consistent with the results of EDX analysis (Table S1). Finally, 1%Rh@C HRTEM images show lattice spacings of 2.3 Å corresponding to the plane (111) of metallic Rh (Figures S13-S18).

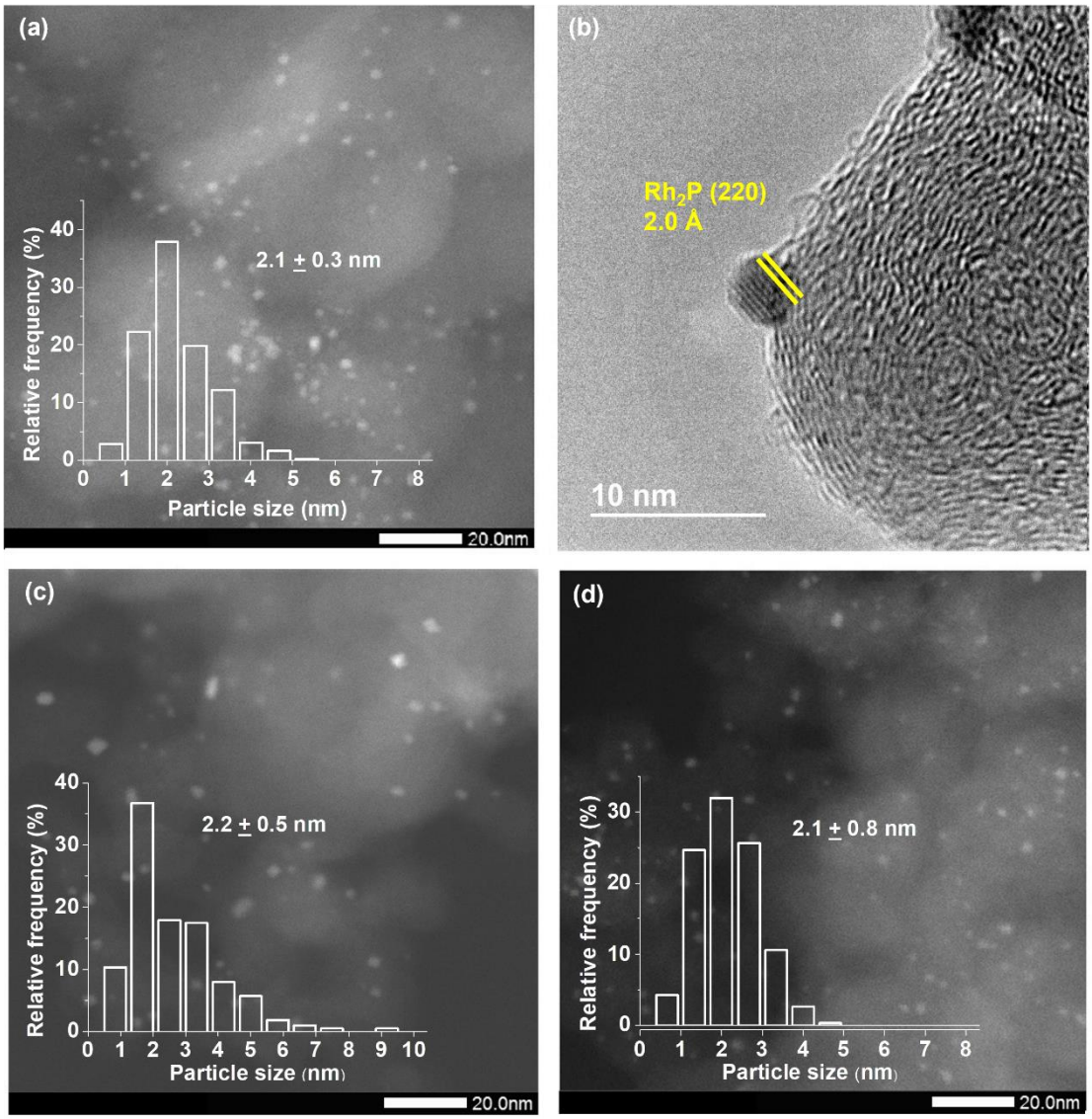

Figure 1. HAADF-STEM images and histograms for: (a) 1%Rh_2P@C, (c) 1%Rh@C, (d) 1%Rh-PPh_3@C. At least 200 nanoparticles were measured for the statistical study. HRTEM image (b) of 1%Rh_2P@C.

XRPD patterns were measured for all catalysts at 1%, but samples at this metal loading barely showed any diffraction peaks related to Rh species due to small particle sizes (<4-5nm),[24] for this reason, catalysts with higher metal loading were also prepared, such as 5%Rh@C (Figure S20), which presents characteristic XRD diffraction peaks at 2θ = 41.0, 47.8, 69.7 and 84.6º for the *fcc* Rh^0 facets (111), (200), (220) and (311), respectively.[25] The peak at 2θ around 25º corresponds to (002) of graphite and the broad peak between 40-46º to (100) plane of disordered graphite. This confirms that the support has a turbostratic structure, which is a mixture of amorphous and graphitic carbon, something typical in carbon blacks.[26,27,28] Conversely, 5%Rh_2P@C (Figure S20) displayed peaks at 2θ = 32.4, 46.6, 57.9, 68.1, 77.6 and 86.9º, which indicates the presence of Rh_2P nanocrystals with (200), (220), (222), (400), (420) and (422) facets being this in concordance with TEM data.[18,29] It appears that the Wilkinson complex is a good source for both metal and phosphorus and that it can promote the selective formation of Rh_2P nanoparticles.

To shed light on the effect of phosphorus on the process, isotopic H/D exchange experiments have been performed on Rh@C and Rh_2P@C, and it was observed that the dissociation of H_2 is faster in Rh_2P@C than in Rh@C. These tests allowed the obtention of HD and H_2 mass signals at room temperature and the ratios between them for catalysts 1%Rh@C and 1%Rh_2P@C, with values of 0.138 and 0.245, respectively. Besides, the role of carbon that comes from the organic ligand has been elucidated by Raman spectroscopy. In order to remove carbon signals caused by the support, $Rh_2P@SiO_2$ was synthesized and its Raman spectrum (Figure S31) is in agreement with our previous observations,[30] consisting in the formation of graphitic carbon layers around the Rh_2P species. This fact could be key in the stabilization of these NPs during catalytic reactions and against overoxidation when in contact with air.[30,31] Finally, to elucidate if carbon in Rh_2P@C material is surrounding the whole Rh_2P nanoparticle in a core-shell or partially covering it in patches, we have carried out CO chemisorption. This experiment shows that only 5% of total Rh is accessible for CO molecules; therefore it indicates that Rh_2P particles are partly enveloped by carbon.

X-ray Photoelectron Spectroscopy (XPS) characterization has been used to provide information about the electronic properties,[24] however, in our case, for the 1% metal loading, signals were hard to detect due to the low metal content. For 1%Rh_2P@C, the Rh region in the XPS spectrum (Figure S26) showed only two 3d characteristic peaks at 307.9 and 314.6 eV. The binding energy of Rh^0 is usually between 307.0-307.4 eV,[14] while Rh^{3+} in Rh_2O_3 is about 308.5 eV, which means that the value for Rh $3d_{5/2}$ at 307.9 eV is too high to be Rh in metallic state and too low to be Rh^{3+}. Since the binding energy is shifted towards higher values, it indicates that Rh in Rh_2P holds a partial positive charge ($Rh^{\delta+}$). The peak at 314.6 eV was assigned to Rh^{3+} $3d_{3/2}$. In the P 2p region, three peaks are shown. Two of them are just slightly above the background noise and have 129.5 and 130.7 eV binding energies, which were assigned to $2p_{3/2}$ and $2p_{1/2}$, respectively. [14,19] P $2p_{3/2}$ has a binding energy of 130.2 eV[20] in the neutral state, suggesting that the peak at 129.5 eV appears because P is partially negatively charged ($P^{\delta-}$) in Rh_2P.[32] The XPS results indicate that in 1%Rh_2P@C in where the Rh is positively and the P is negatively charged, an electron density transfer may occur from Rh to P. Regarding the third peak in the P 2p region at 133.7 eV, it is assigned to oxidized P species formed on the surface of the particle when exposed to air, as also occurs with Rh^{3+}. In the case of 1%Rh@C, Rh $3d_{5/2}$ peak at 307.2 eV was assigned to the metallic state of Rh and the Rh $3d_{3/2}$ peak at 314.6 eV to Rh^{3+}.

The developed materials were characterized by X-ray Absorption Spectroscopy (XAS) at Rh K-edge to gain insights into the electronic structure of Rh atoms and their local environment in the catalyst prepared by different synthesis methods (Figure 2 and Table S3). At first glance, the spectra of the catalysts show different shapes in comparison with Rh foil (Figure 2a), ruling out the presence of metallic nanoparticles in the samples prepared using Rh and P sources. The position of the absorption edge in the catalyst prepared from the Wilkinson complex is 0.5 eV shifted towards higher energies with respect to the Rh foil (23220 eV), pointing out that Rh atoms are discretely oxidized (δ^+), as already indicated by XPS results. Differently, the catalyst prepared by the mixture of $RhCl_3$ and PPh_3 displays mixed spectra between Rh_2P and Rh_2O_3, with absorption edge shifted 1.4 eV to higher energies with respect to the Rh_2P catalyst due to the

presence of the oxidic phase in the sample. Linear combination analysis estimated that Rh-PPh_3@C catalyst is composed of 76% of Rh_2P and 24% of Rh_2O_3 phases (Figure 2a). The Extended X-ray Absorption Fine Structure (EXAFS) spectra of Rh_2P catalyst (inset of Figure 2a) shows mainly three contributions at 1.94, 2.49 and 3.65 Å related to Rh-P, Rh-Rh and Rh-Rh bonds. The Rh-PPh_3@C sample also shows three contributions at the magnitude of the Fourier transform |FT|, namely Rh-O (from Rh_2O_3 phase) at 1.60 Å, a shoulder around 1.9 Å of Rh-P bond and a third one at 2.45 Å from Rh-Rh bond. The near-edge spectra of Rh@C catalysts (Figure 2b) resemble that of Rh^0 standard but with flattened intensity of the first two oscillations beyond the edge (related to Rh *fcc* crystalline phase), which is typical of finite size effects in nanostructured materials.

Notwithstanding, the spectrum of 1%Rh@C sample displays a slightly increased whiteline in comparison to Rh^0 and 5% Rh@C spectra, suggesting that Rh atoms are partially oxidized. This can be further validated by looking at the magnitude of Fourier transform (inset of Figure 2b) of this sample, which, apart from the main Rh-Rh contribution between 2-3 Å, presents a shoulder at ~1.7 Å related to the Rh-O contribution. Moreover, significant flattened EXAFS peaks can be perceived when comparing this spectrum with that of Rh metal, supporting the results from STEM images about the nanosize character of Rh species. More details on EXAFS fittings can be found in Table S3. The quantitative results confirm the formation of an exclusive single phase of Rh_2P in Rh_2P@C material (in agreement with crystallographic data), while Rh-PPh_3@C consists of a mixture of Rh phases particular Rh_2O_3 and Rh_2P. Therefore, the employment of a well-defined metal precursor drives the formation of better materials based on homogeneity, distribution and metallic nature.

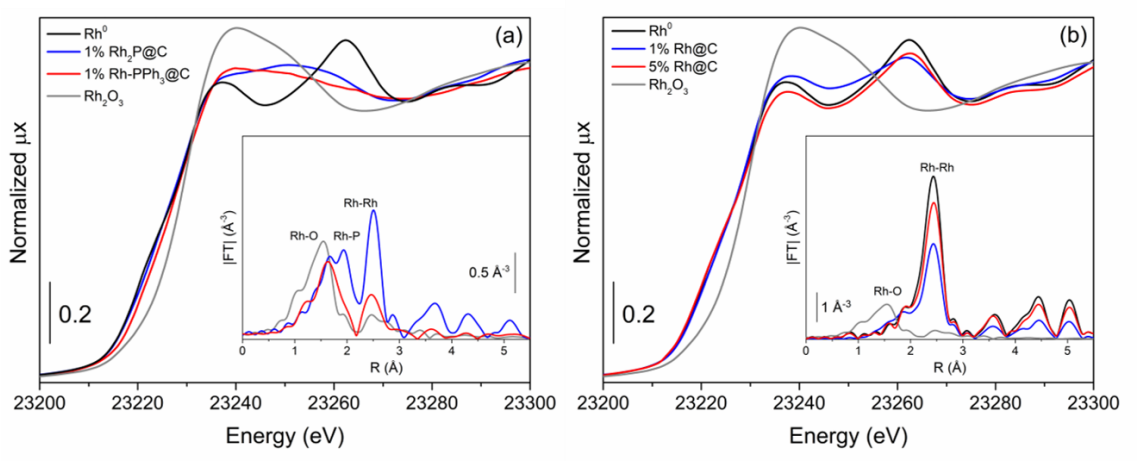

Figure 2. Normalized XANES spectra at Rh K-edge and k^2-weighted |FT| (inset) of Rh_2P@C (a) and Rh@C (b) catalysts.

Rh_2P nanoparticles developed by the two synthetic strategies were assessed in liquid-phase hydroformylation of olefins. The difference between the two of them lies in the Rh and P source, as stated before. In addition, the effect of phosphorus on the catalytic activity and the stability of the material has been studied as opposed to metallic Rh as active species. Finally, these heterogeneous catalysts are compared to a benchmark homogeneous catalyst, the Wilkinson complex.

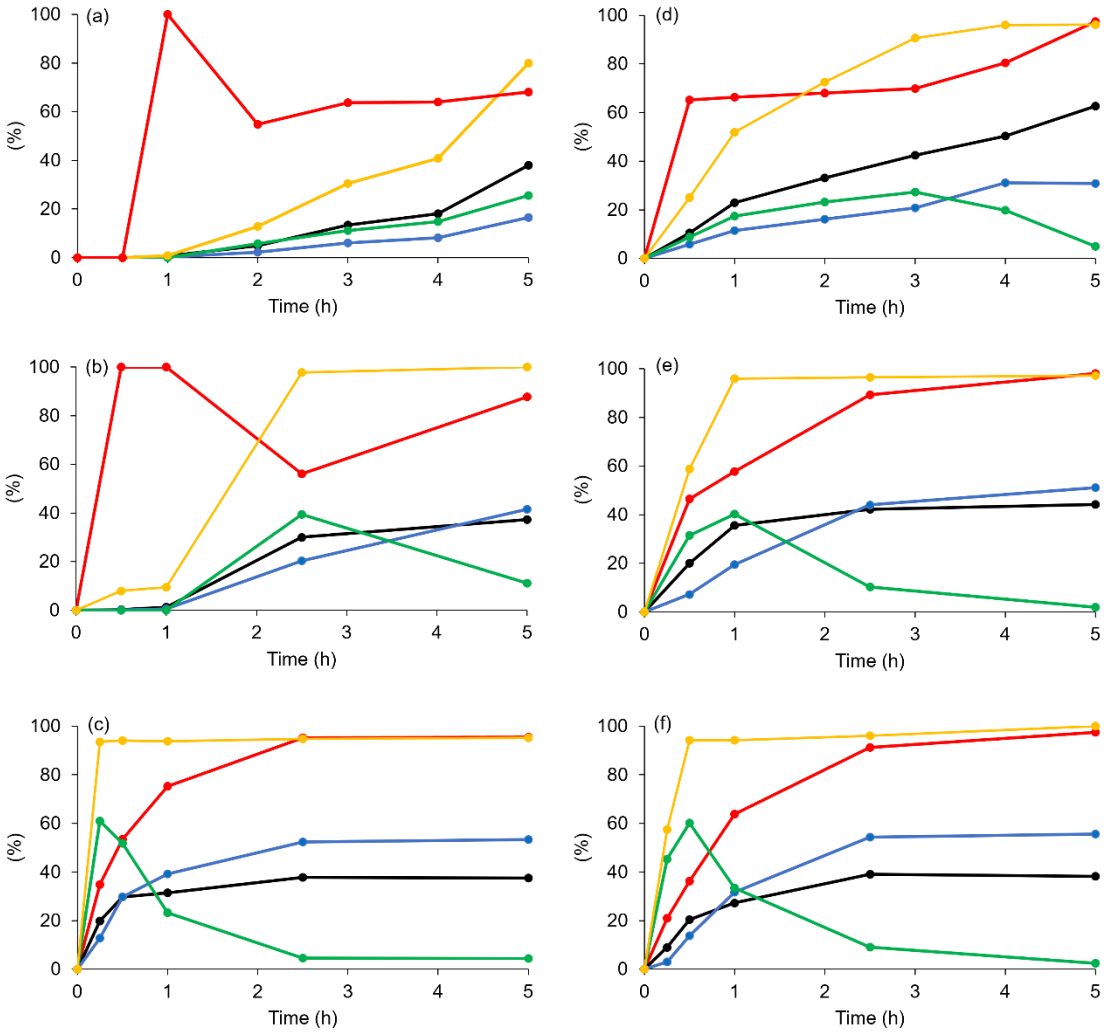

Figure 3. Graphs on the left correspond to $RhCl(PPh_3)_3$ as catalyst at 60 ºC (a), 80 ºC (b) and 100 ºC (c) and to 1%Rh_2P@C on the right at 60 ºC (d), 80 ºC (e) and 100 ºC (f). Plots in red indicate aldehyde selectivity, in black the yield of the linear product, in blue the yield of the branched product, in green the yield of isomerization reaction and in yellow the 1-hexene conversion. Reaction conditions: Rh/olefin 1:500, 1-hexene 1.5 mmol, 1.5 mL toluene, p = 40 bar, H_2/CO = 1:1.

Reactions were performed under 40 bar of syngas pressure (CO:H_2, 1:1) in reaction times of 5 hours, with 1-hexene as model substrate. In our case, apart from isomerization, no hydrogenation products were detected in any case. Reaction kinetics were studied with respect to 1-hexene with 1%Rh_2P@C and the Wilkinson complex as catalysts (Figures 3 & 4, and entries 1-11 of Table 1), and a first-order reaction was determined in both cases. Our first thought was to establish the molecular catalytic result as a benchmark for next tests, nevertheless, it exhibited an activity lower than expected at 60 ºC, with a conversion of 82% and a selectivity of 67% in five hours, which, as kinetic studies revealed, could be caused by longer induction times as it also occurred at 80 ºC.

This induction time of one hour was not observed at 100 ºC. These induction times could be caused by the activation of the Wilkinson complex in the reaction, which needs to undergo ligand exchange between PPh_3 and carbon monoxide, hydrogen addition, apart from the complexation of the alkene. [33]

Regarding 1%Rh_2P@C, no induction times were observed at any temperature within the times on stream considered here, and TOFs were 17788 h^{-1} (0.25 h) at 100 ºC and 5236 h^{-1} (0.5 h) at 60 ºC. These TOF values indicate the high activity of accessible metal centers, which as CO chemisorption tests showed, constitute only the 5% of total rhodium in the material. In comparison with the molecular catalyst, the catalytic result obtained for the heterogeneous catalyst with just a 5% of available rhodium equals (or improves depending on the reaction temperature) the Wilkinson complex with all the metal available. Apparent activation energies (Ea) of 30.8 kJ/mol and 38.5 kJ/mol were obtained for the processes catalysed with 1%Rh_2P@C and the Wilkinson complex, respectively (Figure 4b). The calculation of apparent activation energies is explained in Section 3.8 of the SI together with the values of kinetic constants at different temperatures (Table S5). The similarity in Ea clearly proves that Rh_2P phase is a suitable mimic of $[Rh^{I}(Ph_3P)_3]^{+}$, which could be pivotal in replacing homogeneous catalysts in the hydroformylation of olefins. In this sense, 1%Rh_2P@C is a material with an activity comparable to homogeneous systems with the added advantages of having better conversions at lower temperatures (Figure 4a) and being easily recovered. Ratios of l/b regioisomers are not too high, even at low temperatures, but the l/b ratio decreases when the reaction temperature increases because of the isomerization of 1-hexene to the internal olefin, which leads to the formation of the branched product (Table 1 and Figure 3). In fact, the hydroformylation of internal alkenes is also favoured when the temperature is increased, which helps to enhance the yields to aldehydes (Figure 3). Moreover, at 60 ºC Rh_2P catalyst is more efficient than the Wilkinson one for hydroformylation of these internal alkenes since olefin isomerization is detected during the reactions, but it is consumed, as it has been extracted from kinetic experiments (Figures 3).

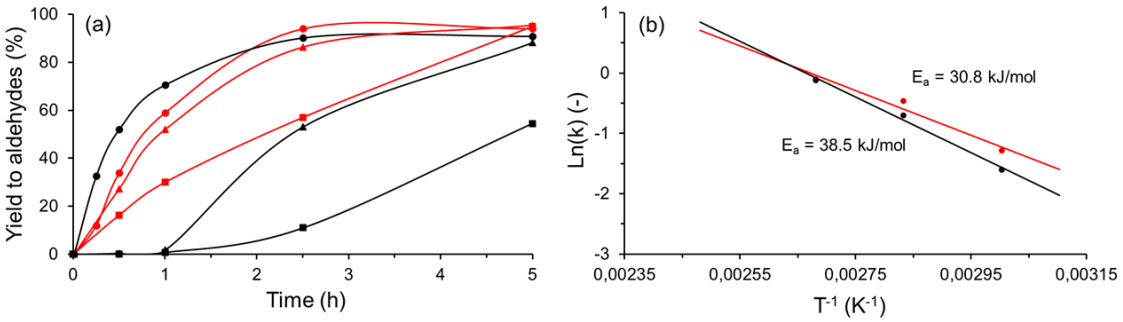

Figure 4. a) Yield to aldehydes using 1%Rh_2P@C and the Wilkinson complex at different temperatures: Wilkinson complex at 100 ºC (black circle), 80 ºC (black triangle) and 60 ºC (black square); 1%Rh_2P@C at 100 ºC (red circle), 80 ºC (red triangle) and 60 ºC (red square). b) Plot for the determination of the apparent activation energy for 1%Rh_2P@C (red) and the Wilkinson complex (black).

Besides, the heterogeneous catalysts developed here were studied and compared with each other (Table 1 and Figure 5). Considering that 1%Rh@C, 1%Rh-PPh_3@C and 1%Rh_2P@C have similar Rh particle sizes and that the last two catalysts show higher conversions than 1%Rh@C (Figure 5a and entries 4-15 of Table 1), we can assure that the difference in the catalytic behaviour cannot be produced by variations in the metal crystalline size but to the presence of phosphorus and its positive effect on the reaction. This could be explained by the fact that in Rh_2P species, Rh holds a partial positive charge that could facilitate the coordination of nucleophilic molecules during the reaction, such as alkenes and CO, which does not apply for the neutral state in metallic Rh, as has been theoretically proposed.[22] In terms of rhodium phosphide catalysts, 1%Rh_2P@C shows a higher yield to aldehydes than 1%Rh-PPh_3@C, this catalytic result is consistent with what was observed in XAS measurements, since 1%Rh-PPh_3@C showed mixed spectra between Rh_2P and Rh_2O_3 phases, whereas 1%Rh_2P@C has revealed a unique Rh_2P phase. Although both synthetic methods provide the formation of Rh_2P nanoparticles active in hydroformylation, the one using $Rh(PPh_3)_3Cl$ as a precursor is the one that selectively generates the Rh_2P active species (Figure 5a).

Table 1. Hydroformylation of 1-hexene on Rh catalysts.[a]

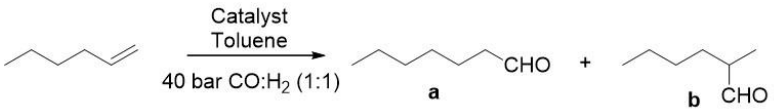

Entry	Catalyst	T[a] (ºC)	Rh:C_6H_{12}	Conversion (%)	Selectivity (%)	ratio l/b	TOF[b] (h^{-1})	TON[b]
1	$RhCl(PPh_3)_3$	60	1:500	82	67	70:30	33[c]	306[c]
2	$RhCl(PPh_3)_3$	80	1:500	100	88	47:53	109[c]	484[c]
3	$RhCl(PPh_3)_3$	100	1:500	95	95	41:59	674[c]	506[c]
4	1%Rh_2P@C	60	1:500	96	94	67:33	3422	9724
5	1%Rh_2P@C	60	1:1000	99	86	57:43	5236	18030
6	1%Rh_2P@C	80	1:500	97	95	47:53	5727	9828
7	1%Rh_2P@C	100	1:500	100	94	41:59	5883	9724
8	1%Rh_2P@C	100	1:1000	100	99	44:56	17788	10241
9	0.5%Rh_2P@C	60	1:1000	100	84	63:37	3000	17379
10	0.3%Rh_2P@C	60	1:1700	98	75	67:33	2865	25862
11	5%Rh_2P@C	60	1:500	77	69	69:31	155	1427
12	1%Rh-PPh_3@C	60	1:500	100	83	55:45	1178	4770
13	5%Rh-PPh_3@C	60	1:500	67	61	69:31	334	701
14	1%Rh@C	60	1:500	63	72	67:33	308	1241
15	5%Rh@C	60	1:500	4	-	-	-	-

[a] Reaction conditions: 40 bar (CO/H_2 = 1:1), 60 ºC, 1.5 mL toluene, 5 hours; [b] TOFs and TONs were calculated considering accessible Rh obtained by CO titration unless otherwise stated, and TOFs were calculated at conversions lower than 20%. [c] TOFs and TONs were calculated based on all the metal present.

After testing Rh_2P catalysts at 1, 0.5 and 0.3% metal loadings, a pattern was observed (Figure 5b and Figure S32); although the rhodium content has been halved and diminished to the third part, the catalytic activity in terms of conversions have not been dramatically affected. This tendency could be explained by the fact that a reduction in the rhodium content causes a decrease in the nanoparticle mean diameter with 2.1 nm, 1.8 and 1.3 nm for 1%Rh_2P@C, 0.5%Rh_2P@C, 0.3%Rh_2P@C, respectively (Figures S1, S4 and S5). The percentage of nanoparticles with an average size below 1 nm is higher at 0.3%, which means that this catalyst could show a different interaction with substrates than its larger counterparts.[34] In fact, a diminution in particle size is usually associated with an increase in the ratio of surface atoms in vertices and edges with regard

to atoms in planes, which could be reflected in the rise of available rhodium atoms for hydroformylation (Figure 5b).[35] In order to shed it, the initial rates for these catalysts normalized to the surface metal atoms have been obtained (Figure S32b); this comparison provides similar values supporting that this reaction is not sensitive to crystal particle size at the metal loadings of 1, 0.5 and 0.3%.

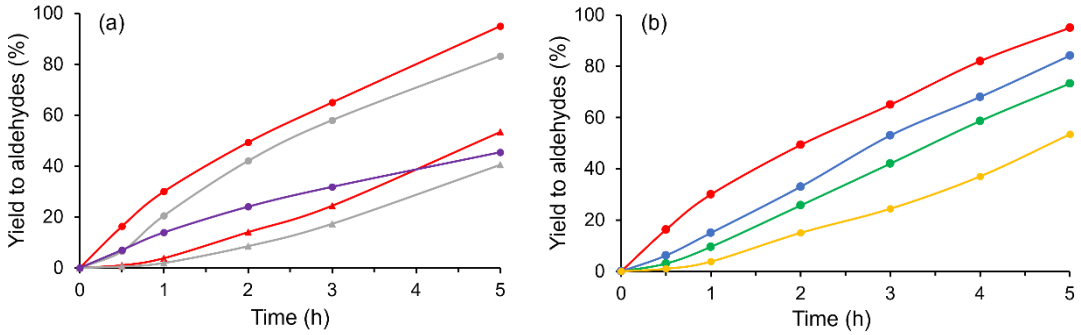

Figure 5. Reaction conditions: Rh/olefin 1:500, 1-hexene 1.5 mmol, 1.5 mL toluene, p = 40 bar, H_2/CO = 1:1, 60ºC. (a) Yield to aldehydes using: 1%Rh_2P@C (red circle), 1%Rh-PPh_3@C (grey circle), 1%Rh@C (purple circle), 5%Rh_2P@C (red triangle), 5%Rh-PPh_3@C (grey triangle). (b) Reaction profiles for 1%Rh_2P@C (red), 0.5%Rh_2P@C (blue), 0.3%Rh_2P@C (green) and 5%Rh_2P@C (yellow).

To go further on the research of the suitability of the material for the liquid-phase hydroformylation reaction and to cover the scope of most studied alkenes (Table 2), besides 1-hexene, 1%Rh_2P@C was tested with other olefins: propylene as short-chain alkene; cyclohexene as internal cyclic and non-isomerizable substrate; styrene as aromatic compound and *n*-octene as a longer chain olefin. 1%Rh_2P@C showed almost total conversion for styrene and propylene, and in the case of the latter, yields for linear and branched products were practically identical because of the absence of steric hindrance in the molecule and thereby, no preferred orientation. On the styrene side, at 60 ºC, the branched aldehyde is predominant, which is in agreement with observations found in other studies, both in molecular and heterogeneous catalysis.[9,22,36,37] In general, yields are excellent, except for cyclohexene, whose result is caused by its internal alkene nature resulting in an added difficulty of approaching the catalytic site, as has been previously detected by other authors. In fact, this is the lowest temperature described up to date for achieving

alkene hydroformylation in liquid phase with heterogeneous catalysts keeping excellent TOF values.

Table 2. Hydroformylation of different olefins using 1%Rh_2P@C as catalyst.[a]

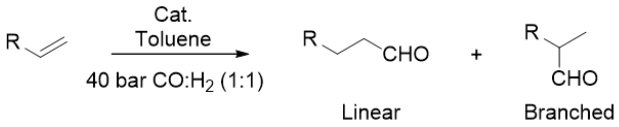

Substrate	Yield to aldehydes (%)	Conversion (%)	l/b
1-hexene	94	96	67:33
Cyclohexene	51	51	-
Styrene	99	99	21:79
1-octene	84	97	62:38
Propylene	98	98	50:50

[a] Reaction conditions: substrate (1.5 mmol), catalyst (30 mg), toluene (1.5 mL), 40 bar ($CO:H_2$), 60 ºC, 5 hours.

In hydroformylation reactions metal leaching is common. In fact, in the presence of CO, metals can be converted into metal carbonyls and be transferred from the support to the solution.[38,39,40] This issue has attracted the attention of researchers in the last years. Fujimoto et al. reported the amounts of metal leached from catalysts supported on active carbon at different syngas pressures. Their results showed leaching dependence on syngas pressure with 20% of metal leached under 3.0 MPa of syngas, and about 50% under 5.0 MPa.[41] Beller et al. reported conversions and quantities of metal leached for catalysts prepared on different supports that proved its influence on leaching.[42] Wen and coworkers recently reported leaching suppression with citric acid, formic acid and oxalic acid as protectants. Leaching was dramatically reduced but at the expense of part of the catalytic activity.[43]

Some studies on Rh nanoparticles applied on hydroformylation and their results from leaching tests were found, but none on Rh_2P nanoparticles. To determine the Rh leaching in our catalysts, solutions were filtered while hot and after sample treatment, the amount of leached Rh was obtained by Inductively Coupled Plasma Mass Spectrometry (ICP-MS analyses), which are

residual quantities for the analysed samples. Then, considering conversion rates, the catalytic activity can be assigned to the heterogeneous component.

Besides, in order to support the heterogeneous nature of the catalysts, twin reactions were carried out. After one hour, one of them was stopped, filtered while hot and put into the reactor again. Samples were taken simultaneously in both filtered and non-filtered reactions at reaction times of 1 and 5 hours. Then, progress in the reaction after 4 hours (Figure 6a), is marginal when compared to the conversion rate obtained for the non-filtered reaction (Figure 6a).

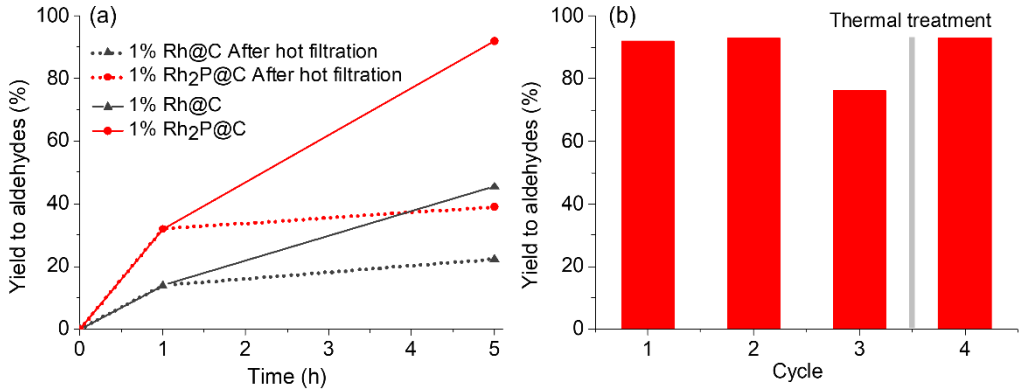

Figure 6. Reaction conditions: Rh/olefin 1:500, 1-hexene 1.5 mmol, 1.5 mL toluene, p = 40 bar, H_2/CO = 1:1, 60 ºC (a) Reaction profiles of 1%Rh_2P@C (red) and 1%Rh@C (black) with (dot line) or without (straight line) hot filtration. (b) Conversions for 1% Rh_2P@C over the course of four reaction cycles.

Studies on the stability of the material were completed with recycling tests; in Figure 6b, yields for the successive reaction runs are represented. 1%Rh_2P@C shows good yields during four catalytic cycles and an unchanged selectivity. However, there is a decline in the catalytic activity at the third run, with a product yield of 72% instead of 94% in the first use. One of the possible reasons for this fact is particle growth, however, particles only underwent a slight growth after three catalytic cycles from 2.1 nm to 2.3 nm, so this is unlikely to be the cause for the decrease in the catalytic activity (Figure 7). Another reason that can explain this behaviour is the adsorption of reaction products on the catalyst surface, which was later confirmed when the catalyst recovered the initial activity after calcination at 300 ºC under air (Figure 6b).[31] Nevertheless, to ascertain that there are no changes in the structure during catalytic conditions, 5%Rh_2P@C, 1%Rh_2P@C, 1%Rh-PPh_3@C and 1%Rh@C were characterized by XRD, HAADF-STEM,

HRTEM, XPS and XAS after catalysis. 5%Rh_2P@C XRD pattern shows high crystallinity after catalysis (Figure S21), and the diffractograms obtained for the catalyst at 1% metal loading do not reveal any significant particle growth, which is in agreement with particle size measurements, since the material that experienced more particle development is 1%Rh@C, from 2.2 to 2.8 nm (Figure 7). However, in the XRD diffractogram of post-catalysis 1%Rh-PPh_3@C (Figure S23), there is a little peak at 48.7º attributed to Rh_2P (220), which could reveal some formation of small aggregates during catalysis that were not observed in HRTEM images (Figure 7b). Regarding XPS measurements of the materials after catalysis, they did not present any changes. In addition, HRTEM post-reaction images of 1%Rh_2P@C, 1%Rh-PPh_3@C and 1%Rh@C showed no alterations in the crystalline structure (Figures S14, S16 and S17).

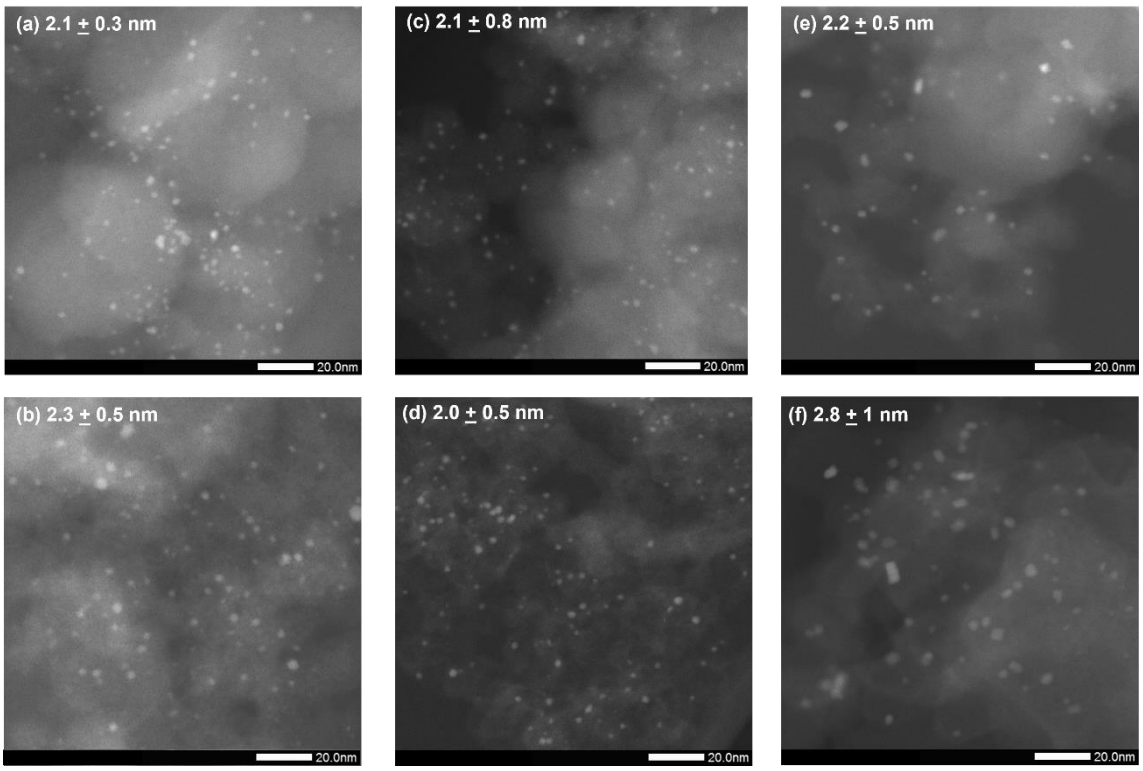

Figure 7. HAADF-STEM images of: 1%Rh_2P@C before (a) and after three catalysis runs (b), 1%Rh-PPh_3@C before (c) and after one catalysis run (d); 1%Rh@C before (e) and after one catalysis run (f).

Figure 8 shows the XAS results of Rh_2P@C and Rh@C catalysts before and after catalysis. The spectrum of 1% Rh_2P@C slightly changed post-reaction with almost no perceptible differences

in XANES while that of 1% Rh-PPh_3@C showed an increased whiteline which indicates that Rh atoms are even more oxidized after reaction conditions (Figure 8a). Linear combination analysis showed that Rh_2O_3 fraction increased from 24 to 28% in the Rh-PPh_3@C sample after reaction (Figure S27). A slight increase of the higher-shell contributions in the |FT| of 1%Rh_2P@C catalyst spectrum can be seen (Figure 8), suggesting some minor particle sintering. This is also observed in the spectrum of 1%Rh-PPh_3@C, which also displays a minor increase in the magnitude of |FT| peaks, which is correlated with its XRD spectra (Figure S24). The absorption edge in the XANES spectrum of 1%Rh@C after catalysis (Figure 8c) slightly shifts towards higher energies (from 23220.5 to 23221 eV) as well as the intensity of whiteline increases, indicating that a portion of Rh atoms is being oxidized after reaction. Linear combination analysis (Figure S28) shows an increase of ~12% in this oxidized phase with respect to the sample before catalysis. This can also be observed in the |FT| where the first-shell peak at ~1.6 Å, related to Rh-O contribution, gain intensity with respect to the as-prepared sample, supporting Rh atoms are being oxidized. Moreover, the Rh-Rh contribution at 2.4 Å slightly flattens in intensity (from 3.17 to 2.55 $Å^{-3}$) due to the decrease of the metallic character in the sample. These results reinforce the role of phosphorus in the stability of the catalysts presented herein once very subtle changes are observed in the XAS spectra after hydroformylation reactions.

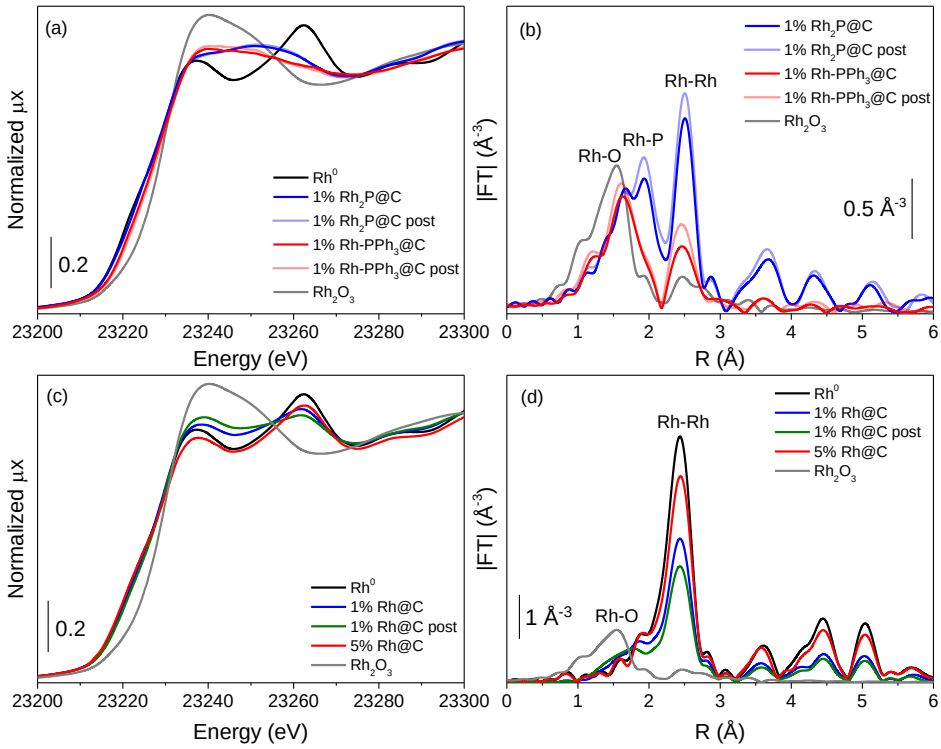

Figure 8. Normalized XANES spectra at Rh K-edge (a,c) and k^2-weighted |FT| (b,d) of Rh_2P@C and Rh@C catalysts before and after catalysis.

Conclusions

This study demonstrates that it is possible to obtain well-defined supported Rh_2P nanoparticles by introducing Rh and P from a definite Rh-P transition metal complex (the Wilkinson complex), followed by pyrolysis in a N_2 atmosphere. The surface species formed are ascertained by a combination of spectroscopic techniques, including XAS, whose application to the characterization of Rh_2P species is uncommon and whose results reveal the high purity of the synthesized Rh_2P nanoparticles and their stability during reaction conditions. The species formed here are very active and selective for catalysing the hydroformylation of olefins at low temperatures, as the outstanding TOFs have shown. Remarkably, the catalytic results achieved with the supported Rh_2P nanoparticles are in the same level of transition metal complexes. This indicates that we have a high-performing Rh heterogeneous catalyst for hydroformylation reactions. The key point for this outperforming catalytic behaviour is the Rh and P interaction when conforming the Rh_2P catalytically active species.

Associated content

Supporting Information

Catalyst preparation; catalytic tests conditions; equipment spectifications; HAADF-STEM and HRTEM images of catalysts before and after catalysis; EDX analysis results,; XRPD, XPS, XAS and Raman spectra; catalytic plots; kinectic constants calculation.

Author information

Corresponding author

Pascual Oña-Burgos: *pasoabur@upvnet.upv.es;* ORCID: 0000-0002-2341-7867

Notes

The authors declare no competing financial interest.

Acknowledgments

Program Severo Ochoa SEV-2016-0683 is gratefully acknowledged. C.G.R. thanks to MINECO for her FPU Ph.D. contract FPU17/04172. The authors thank the financial support by the Spanish Government (RTI2018-096399-A-I00). The authors thank J.G.M. for his technical support. We also thank the Electron Microscopy Service of the UPV for TEM facilities. C.W.L. thanks PRH 50.1 – ANP/FINEP Human Resources Program for the Visiting Researcher Fellowship. This research used resources of the Advanced Photon Source, an Office of Science User Facility operated for the U.S. Department of Energy (DOE) Office of Science by Argonne National Laboratory and was supported by the U.S. DOE under Contract No. DE-AC02-06CH11357, and the Canadian Light Source and its funding partners.

References

(1) Franke, R.; Selent, D.; Börner, A. Applied Hydroformylation. *Chem. Rev.* **2012**, *112*, 5675–5732.

(2) Breit, B.; Seiche, W. Recent Advances on Chemo-, Regio- and Stereoselective Hydroformylation. *Synthesis (Stuttg).* **2001**, *1*, 1–36.

(3) Li, C.; Wang, W.; Yan, L.; Ding, Y. A Mini Review on Strategies for Heterogenization of Rhodium-Based Hydroformylation Catalysts. *Front. Chem. Sci. Eng.* **2018**, *12*, 113–123.

(4) Tan, M.; Yang, G.; Wang, T.; Vitidsant, T.; Li, J.; Wei, Q.; Ai, P.; Wu, M.; Zheng, J.; Tsubaki, N. Active and Regioselective Rhodium Catalyst Supported on Reduced Graphene Oxide for 1-Hexene Hydroformylation. *Catal. Sci. Technol.* **2016**, *6*, 1162–1172.

(5) Sun, Q.; Dai, Z.; Liu, X.; Sheng, N.; Deng, F.; Meng, X.; Xiao, F. S. Highly Efficient Heterogeneous Hydroformylation over Rh-Metalated Porous Organic Polymers: Synergistic Effect of High Ligand Concentration and Flexible Framework. *J. Am. Chem. Soc.* **2015**, *137*, 5204–5209.

(6) Li, C.; Yan, L.; Lu, L.; Xiong, K.; Wang, W.; Jiang, M.; Liu, J.; Song, X.; Zhan, Z.; Jiang, Z.; Ding, Y. Single Atom Dispersed Rh-Biphephos&PPh_3@porous Organic Copolymers: Highly Efficient Catalysts for Continuous Fixed-Bed Hydroformylation of Propene. *Green Chem.* **2016**, *18*, 2995–3005.

(7) Gorbunov, D.; Safronova, D.; Kardasheva, Y.; Maximov, A.; Rosenberg, E.; Karakhanov, E. New Heterogeneous Rh-Containing Catalysts Immobilized on a Hybrid Organic-Inorganic Surface for Hydroformylation of Unsaturated Compounds. *ACS Appl. Mater. Interfaces* **2018**, *10*, 26566–26575.

(8) Li, P.; Thitsartarn, W.; Kawi, S. Highly Active and Selective Nanoalumina-Supported Wilkinson's Catalysts for Hydroformylation of Styrene. *Ind. Eng. Chem. Res.* **2009**, *48*, 1824–1830.

(9) Amsler, J.; Sarma, B. B.; Agostini, G.; Prieto, G.; Plessow, P. N.; Studt, F. Prospects of Heterogeneous Hydroformylation with Supported Single Atom Catalysts. *J. Am. Chem. Soc.* **2020**, *142*, 5087–5096.

(10) Wang, L.; Zhang, W.; Wang, S.; Gao, Z.; Luo, Z.; Wang, X.; Zeng, R.; Li, A.; Li, H.; Wang, M.; Zheng, X.; Zhu, J.; Zhang, W.; Ma, C.; Si, R.; Zeng, J. Atomic-Level Insights in Optimizing Reaction Paths for Hydroformylation Reaction over Rh/CoO Single-Atom Catalyst. *Nat. Commun.* **2016**, *7*, 1–8.

(11) Lang, R.; Li, T.; Matsumura, D.; Miao, S.; Ren, Y.; Cui, Y. T.; Tan, Y.; Qiao, B.; Li, L.; Wang, A.; Wang, X.; Zhang, T. Hydroformylation of Olefins by a Rhodium Single-Atom Catalyst with Activity Comparable to $RhCl(PPh_3)_3$. *Angew. Chemie - Int. Ed.* **2016**, *55*, 16054–16058.

(12) Griffin, M. B.; Baddour, F. G.; Habas, S. E.; Ruddy, D. A.; Schaidle, J. A. Evaluation of Silica-Supported Metal and Metal Phosphide Nanoparticle Catalysts for the Hydrodeoxygenation of Guaiacol under Ex Situ Catalytic Fast Pyrolysis Conditions. *Top. Catal.* **2016**, *59*, 124–137.

(13) Habas, S. E.; Baddour, F. G.; Ruddy, D. A.; Nash, C. P.; Wang, J.; Pan, M.; Hensley, J. E.; Schaidle, J. A. A Facile Molecular Precursor Route to Metal Phosphide Nanoparticles and Their Evaluation as Hydrodeoxygenation Catalysts. *Chem. Mater.* **2015**, *27*, 7580–7592.

(14) Hayes, J. R.; Bowker, R. H.; Gaudette, A. F.; Smith, M. C.; Moak, C. E.; Nam, C. Y.; Pratum, T. K.; Bussell, M. E. Hydrodesulfurization Properties of Rhodium Phosphide: Comparison with Rhodium Metal and Sulfide Catalysts. *J. Catal.* **2010**, *276*, 249–258.

(15) Kanda, Y.; Matsukura, Y.; Sawada, A.; Sugioka, M.; Uemichi, Y. Low-Temperature Synthesis of Rhodium Phosphide on Alumina and Investigation of Its Catalytic Activity toward the Hydrodesulfurization of Thiophene. *Appl. Catal. A Gen.* **2016**, *515*, 25–31.

(16) Kanda, Y.; Temma, C.; Sawada, A.; Sugioka, M.; Uemichi, Y. Formation of Active Sites and Hydrodesulfurization Activity of Rhodium Phosphide Catalyst: Effect of Reduction Temperature and Phosphorus Loading. *Appl. Catal. A Gen.* **2014**, *475*, 410–419.

(17) Kanda, Y.; Temma, C.; Nakata, K.; Kobayashi, T.; Sugioka, M.; Uemichi, Y. Preparation and Performance of Noble Metal Phosphides Supported on Silica as New Hydrodesulfurization Catalysts. *Appl. Catal. A Gen.* **2010**, *386*, 171–178.

(18) Yang, F.; Zhao, Y.; Du, Y.; Chen, Y.; Cheng, G.; Chen, S.; Luo, W. A Monodisperse Rh_2P-Based Electrocatalyst for Highly Efficient and pH-Universal Hydrogen Evolution Reaction. *Adv. Energy Mater.* **2018**, *8*, 1–7.

(19) Wang, K.; Huang, B.; Lin, F.; Lv, F.; Luo, M.; Zhou, P.; Liu, Q.; Zhang, W.; Yang, C.; Tang, Y.; Yang, Y.; Wang, W.; Wang, H.; Guo, S. Wrinkled Rh_2P Nanosheets as Superior pH-Universal Electrocatalysts for Hydrogen Evolution Catalysis. *Adv. Energy Mater.* **2018**, *8*, 1–7.

(20) Duan, H.; Li, D.; Tang, Y.; He, Y.; Ji, S.; Wang, R.; Lv, H.; Lopes, P. P.; Paulikas, A. P.; Li, H.; Mao, S. X.; Wang, C.; Markovic, N. M.; Li, J.; Stamenkovic, V. R.; Li, Y. High-Performance Rh_2P Electrocatalyst for Efficient Water Splitting. *J. Am. Chem. Soc.* **2017**, *139*, 5494–5502.

(21) Alvarado Rupflin, L.; Mormul, J.; Lejkowski, M.; Titlbach, S.; Papp, R.; Gläser, R.; Dimitrakopoulou, M.; Huang, X.; Trunschke, A.; Willinger, M. G.; Schlögl, R.; Rosowski, F.; Schunk, S. A. Platinum Group Metal Phosphides as Heterogeneous Catalysts for the Gas-Phase Hydroformylation of Small Olefins. *ACS Catal.* **2017**, *7*, 3584–3590.

(22) Liu, B.; Huang, N.; Wang, Y.; Lan, X.; Wang, T. Promotion of Inorganic Phosphorus on Rh Catalysts in Styrene Hydroformylation: Geometric and Electronic Effects. *ACS Catal.* **2021**, 1787–1796.

(23) Gutiérrez-Tarriño, S.; Rojas-Buzo, S.; Lopes, C. W.; Agostini, G.; Calvino, J. J.; Corma, A.; Oña-Burgos, P. Cobalt Nanoclusters Coated with N-Doped Carbon for Chemoselective Nitroarene Hydrogenation and Tandem Reactions in Water. *Green Chem.* **2021**. https://doi.org/10.1039/d1gc00706h.

(24) Wilde, C. A.; Ryabenkova, Y.; Firth, I. M.; Pratt, L.; Railton, J.; Bravo-Sanchez, M.; Sano,

N.; Cumpson, P. J.; Coates, P. D.; Liu, X.; Conte, M. Novel Rhodium on Carbon Catalysts for the Oxidation of Benzyl Alcohol to Benzaldehyde: A Study of the Modification of Metal/Support Interactions by Acid Pre-Treatments. *Appl. Catal. A Gen.* **2019**, *570*, 271–282.

(25) Kundu, M. K.; Mishra, R.; Bhowmik, T.; Barman, S. Rhodium Metal-Rhodium Oxide (Rh-Rh_2O_3) Nanostructures with Pt-like or Better Activity towards Hydrogen Evolution and Oxidation Reactions (HER, HOR) in Acid and Base: Correlating Its HOR/HER Activity with Hydrogen Binding Energy and Oxophilicity of the Cat. *J. Mater. Chem. A* **2018**, *6*, 23531–23541.

(26) Dandekar, A.; Baker, R. T. K.; Vannice, M. A. Characterization of Activated Carbon, Graphitized Carbon Fibers and Synthetic Diamond Powder Using TPD and DRIFTS. *Carbon N. Y.* **1998**, *36*, 1821–1831.

(27) Lázaro, M. J.; Calvillo, L.; Celorrio, V.; Pardo, J. I.; Perathoner, S.; Moliner, R. Study and Application of Carbon Black Vulcan XC-72R in Polymeric Electrolyte Fuel Cells. *Carbon Black Prod. Prop. Uses* **2011**, 41–68.

(28) Sajjadi, S. A.; Mohammadzadeh, A.; Tran, H. N.; Anastopoulos, I.; Dotto, G. L.; Lopičić, Z. R.; Sivamani, S.; Rahmani-Sani, A.; Ivanets, A.; Hosseini-Bandegharaei, A. Efficient Mercury Removal from Wastewater by Pistachio Wood Wastes-Derived Activated Carbon Prepared by Chemical Activation Using a Novel Activating Agent. *J. Environ. Manage.* **2018**, *223*, 1001–1009.

(29) Zhao, Y.; Jia, N.; Wu, X. R.; Li, F. M.; Chen, P.; Jin, P. J.; Yin, S.; Chen, Y. Rhodium Phosphide Ultrathin Nanosheets for Hydrazine Oxidation Boosted Electrochemical Water Splitting. *Appl. Catal. B Environ.* **2020**, *270*, 118880.

(30) Liu, L.; Gao, F.; Concepción, P.; Corma, A. A New Strategy to Transform Mono and Bimetallic Non-Noble Metal Nanoparticles into Highly Active and Chemoselective Hydrogenation Catalysts. *J. Catal.* **2017**, *350*, 218–225.

(31) Liu, L.; Concepción, P.; Corma, A. Non-Noble Metal Catalysts for Hydrogenation: A

Facile Method for Preparing Co Nanoparticles Covered with Thin Layered Carbon. *J. Catal.* **2016**, *340*, 1–9.

(32) Yang, F.; Zhao, Y.; Du, Y.; Chen, Y.; Cheng, G.; Chen, S.; Luo, W. A Monodisperse Rh_2P-Based Electrocatalyst for Highly Efficient and PH-Universal Hydrogen Evolution Reaction. *Adv. Energy Mater.* **2018**, *8*, 1703489.

(33) Kamer, P. C. J.; Reek, J. N. H.; van Leeuwen, P. W. N. M. Rhodium Catalyzed Hydroformylation. *Mech. Homog. Catal. A Spectrosc. Approach* **2005**, 231–269.

(34) Liu, L.; Corma, A. Metal Catalysts for Heterogeneous Catalysis: From Single Atoms to Nanoclusters and Nanoparticles. *Chem. Rev.* **2018**, *118*, 4981–5079.

(35) Shylesh, S.; Hanna, D.; Mlinar, A.; Kŏng, X. Q.; Reimer, J. A.; Bell, A. T. In Situ Formation of Wilkinson-Type Hydroformylation Catalysts: Insights into the Structure, Stability, and Kinetics of Triphenylphosphine- and Xantphos-Modified Rh/SiO_2. *ACS Catal.* **2013**, *3*, 348–357.

(36) Amsler, J.; Sarma, B. B.; Agostini, G.; Prieto, G.; Plessow, P. N.; Studt, F. Prospects of Heterogeneous Hydroformylation with Supported Single Atom Catalysts. *J. Am. Chem. Soc.* **2020**, *142*, 5087–5096.

(37) Lazzaroni, R.; Raffaelli, A.; Settambolo, R.; Bertozzi, S.; Vitulli, G. Regioselectivity in the Rhodium-Catalyzed Hydroformylation of Styrene as a Function of Reaction Temperature and Gas Pressure. *J. Mol. Catal.* **1989**, *50*, 1–9.

(38) Román-Martínez, M. C.; Díaz-Auñón, J. A.; Salinas-Martínez De Lecea, C.; Alper, H. Rhodium-Diphosphine Complex Bound to Activated Carbon: An Effective Catalyst for the Hydroformylation of 1-Octene. *J. Mol. Catal. A Chem.* **2004**, *213*, 177–182.

(39) Lenarda, M.; Storaro, L.; Ganzerla, R. Hydroformylation of Simple Olefins Catalyzed by Metals and Clusters Supported on Unfunctionalized Inorganic Carriers. *J. Mol. Catal. A Chem.* **1996**, *111*, 203–237.

(40) Díaz-Auñón, J. A.; Román-Martínez, M. C.; Salinas-Martínez De Lecea, C. [Rh(μ-Cl)(COD)]$_2$ Supported on Activated Carbons for the Hydroformylation of 1-Octene: Effects of Support Surface Chemistry and Solvent. *J. Mol. Catal. A Chem.* **2001**, *170*, 81–93.

(41) Li, B.; Li, X.; Asami, K.; Fujimoto, K. Low-Pressure Hydroformylation of Middle Olefins over Co and Rh Supported on Active Carbon Catalysts. *Energy and Fuels* **2003**, *17*, 810–816.

(42) Hertrich, M. F.; Scharnagl, F. K.; Pews-Davtyan, A.; Kreyenschulte, C. R.; Lund, H.; Bartling, S.; Jackstell, R.; Beller, M. Supported Cobalt Nanoparticles for Hydroformylation Reactions. *Chem. - A Eur. J.* **2019**, *25*, 5534–5538.

(43) Zhao, J.; He, Y.; Wang, F.; Zheng, W.; Huo, C.; Liu, X.; Jiao, H.; Yang, Y.; Li, Y.; Wen, X. Suppressing Metal Leaching in a Supported Co/SiO_2 Catalyst with Effective Protectants in the Hydroformylation Reaction. *ACS Catal.* **2020**, *10*, 914–920.

Table of Contents

In this work, single phase Rh_2P nanoparticles stabilized by patches of carbon layers are obtained by the employment of a well-defined molecular complex as unique source of phosphorus and rhodium. Moreover, the final material has shown an excellent catalytic activity and stability for the hydroformylation of olefins, with a performance comparable to that of the benchmark homogeneous catalyst.